Results in Physics 8 (2018) 955–962

Contents lists available at ScienceDirect

Results in Physics

journal homepage: www.journals.elsevier.com/results-in-physics

# Study of electric field distorted by space charges under positive lightning impulse voltage

Zezhong Wang [a,*], Yinan Geng [b]

[a] State Key Laboratory of Control and Simulation of Power Systems and Generation Equipment, Department of Electrical Engineering, Tsinghua University, 100084 Beijing, China
[b] Institute of Nuclear and New Energy Technology, Tsinghua University, 100084 Beijing, China

ARTICLE INFO

*Article history:*
Received 14 October 2017
Received in revised form 15 January 2018
Accepted 15 January 2018
Available online 31 January 2018

*Keywords:*
Streamer
Space charge
Laplace electric field
Poisson electric field
Space charge model

ABSTRACT

Actually, many insulation problems are related to electric fields. And measuring electric fields is an important research topic of high-voltage engineering. In particular, the electric field distortion caused by space charge is the basis of streamer theory, and thus quantitatively measuring the Poisson electric field caused by space charge is significant to researching the mechanism of air gap discharge. In this paper, we used our photoelectric integrated sensor to measure the electric field distribution in a 1-m rod-plane gap under positive lightning impulse voltage. To verify the reliability of this quantitative measurement, we compared the measured results with calculated results from a numerical simulation. The electric-field time domain waveforms on the axis of the 1-m rod-plane out of the space charge zone were measured with various electrodes. The Poisson electric fields generated by space charge were separated from the Laplace electric field generated by applied voltages, and the amplitudes and variations were measured for various applied voltages and at various locations. This work also supplies the feasible basis for directly measuring strong electric field under high voltage.



## Introduction

As the power industry continues to develop around the globe, the voltage of the power grid is increasing. Now that ultra-high-voltage (UHV) transmission is being used, the insulation problem and electrical discharge in air gaps has become a research hotspot [1,28–32]. The most widely used insulating medium is air, which can usually withstand the switching impulse voltage or lightning impulse voltage without breakdown, particularly for positive impulse voltage. Many experiments [2–5] have led to some understanding of the discharge mechanism of the air gap, including streamer discharge and leader discharge. Under a positive impulse voltage, the main contributor to developing continuous discharge is the electric field distortion caused by space charge. Initially, space charge could only be simulated by a point charge or a ring charge [6], but these two models do not accurately represent the measured space charge distribution. Researchers have combined discharge images captured with many methods in order to establish a space charge model that considers spatial distribution [7,8]. However, no matter the kind of space charge model, the model must be verified, and the most direct, effective way to verify a space charge model is to compare its calculated results with the measured electric field distortion caused by space charge.

Initially, researchers measured the space electric field by using a metal ball as a probe, based on the simple, clear capacitive divider principle [9]. However, the metal probe itself distorted the electric field, and the probe's large volume affected its measurement accuracy. Other researchers have used a flux meter to measure the electric field around a grounding electrode, using these measurements to predict and calculate the space electric field. For example, the Renardières group used a flux meter but did not directly measure the space electric field [3]. As integrated optical technology has matured since the 1970s, photoelectric integrated sensors have been increasingly researched. A photoelectric integrated electric-field sensor based on a Mach–Zehnder interferometer [10,11] has been successfully used in aviation and other fields. Recently, an electric-field sensor based on the photoelectric effect was used to measure changes in electric field under an impulse voltage: Hidaka et al. measured the space electric field in a rod–plate air gap of 1–3 m under a switching impulse voltage, obtaining the electric field at the end of the streamer [12,13].

In the present paper, we designed an electric-field sensor based on the Pockels photoelectric effect [14–18]: when the plane polarized light propagates along the optical axis of the piezoelectric crystal in the applied electric field, double refraction occurs, and

* Corresponding author.
*E-mail address:* 181926120@qq.com (Z. Wang).

https://doi.org/10.1016/j.rinp.2018.01.037
2211-3797/

the difference between the two principal refractive indices is proportional to the intensity of the applied electric field. We measured the space electric field in a 1-m rod–plate air gap under positive lightning impulse voltage and measured the Poisson field formed by the space charge. Then we changed the applied voltage and the position of the electric-field sensor, and obtained the changes in regularity of the Poisson field caused by the space charge, which establishes a foundation for building and verifying a space charge model.

## Experimental arrangement

### *Transient electric-field sensor*

In the experiment, the transient electric field of the discharge was measured by our developed photoelectric sensor, which uses the common path interference structure and has good measurement sensitivity as well as temperature and humidity stability. The internal structure of the electric field sensor is shown in Fig. 1. It is based on the chip of lithium niobate crystal which has large thermoelectric, piezoelectric, electro-optic, elasto-optic coefficient and strong photorefractive effect. On the $LiNbO_3$ (chemical expression of lithium niobate) wafer, there are two electrodes and one optical waveguide. The optical waveguide is a dielectric device that guides light propagating inside it. The function of two electrodes is to enhance the magnitude of field induced inside the sensor, which are both placed at several microns from the optical waveguide. Two pieces of silicon are used to increase the reliability of the coupling and splicing of fiber and waveguide. Due to the Pockels effect [17], the electric field to be measured can cause the change of crystal refractive index and the propagation velocity of polarized light in the vertical and horizontal directions become different. Those lead to the phase difference of the output and the electric field is obtained by detecting the phase difference of the output.

The maximum measurable field of the sensor reaches the MV/m regime, its 3 dB upper cut-off frequency is greater than 100 MHz, and its lower cut-off frequency is about 5 Hz. As such, the sensor is well suited to broadband measurement of the strong transient space charge field under the temperature and humidity conditions of our experiment. The dimension of the encapsulated shell of the sensor is 50 × 15 × 8 mm, as shown in Fig. 2.

The photoelectric system used to measure the electric field consists of a laser source, a polarization-maintaining fiber, a polarizer, a polarizing beam splitter, a single-mode fiber, a receiver, and an oscilloscope, as shown in Fig. 3. In this system, the laser source is a photoelectric superluminescent light-emitting diode (SLED) 1310-nm light source (Beijing Conquer Optics Science & Technology Corporation), the optical receiver is a broadband receiver (Agilent 11982A), and the lengths of the polarization-maintaining fiber and single-mode fiber are 50 m. To ensure that the input of sensor

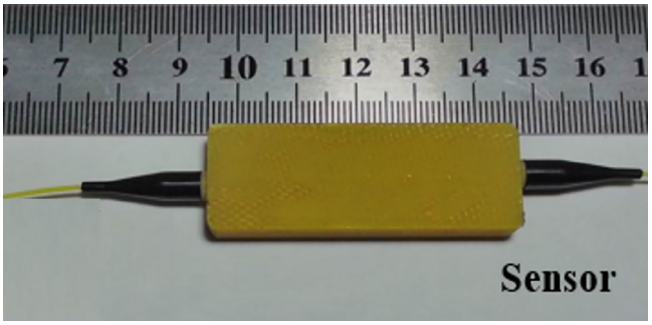


**Fig. 2.** Photograph of the packaged photoelectric field sensor.

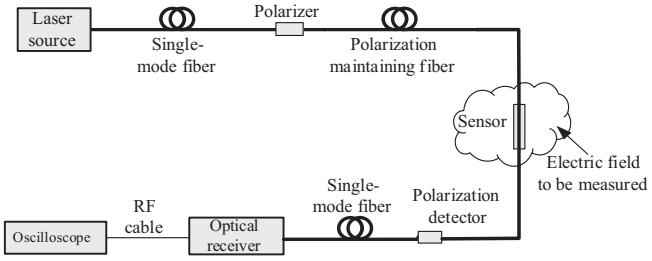


**Fig. 3.** Schematic of the photoelectric system used to measure electric field.

is strictly linearly polarized, a polarizer was added in front of the sensor. The output of the sensor is used to separate the two orthogonal modes with a polarizing beam splitter. The time-domain waveform of the electric field to be measured is passed through the single-mode fiber to the optical receiver, which then transmits it to the oscilloscope. Coupling the sensor with this optical fiber makes it easier to arrange the system so the electric field can be measured at many positions.

### *Setup of the measurement system*

As shown in Fig. 5, the main part of gap discharge is the 1-m rod–plate air gap. To study how the curvature radius of the rod electrode affected the space electric field, as shown in Fig. 4 , we designed metal electrodes with three shapes: cone, hemisphere, and sphere. The metal rod has a length of 60 cm and a radius of 1 cm. The area of the grounding plate is 3 m∗3 m. The lightning impulse voltage generator produces a positive lightning impulse voltage of 100–400 kV with a 2.5-μs wave front time and a 50-μs half-wave time. This voltage is measured by a capacitive divider with a voltage ratio of 1937.5:1. The error of the voltage ratio is smaller than 1% and the square wave response time is 50 ns, which completely satisfies the needs of the lightning impulse voltage measurement.

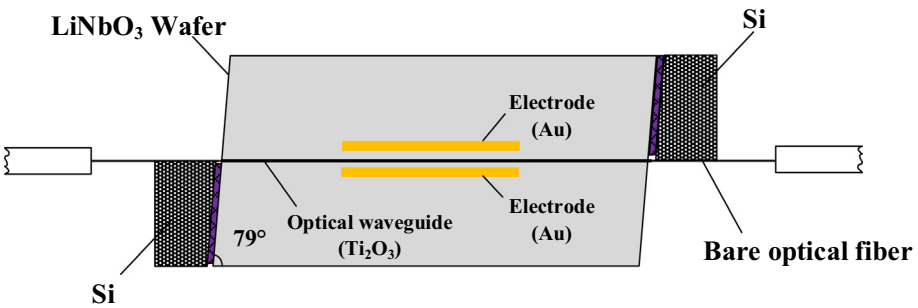


**Fig. 1.** Internal structure of electric field sensor. The electrode is made of gold and the optical waveguide is made from titanium oxide.

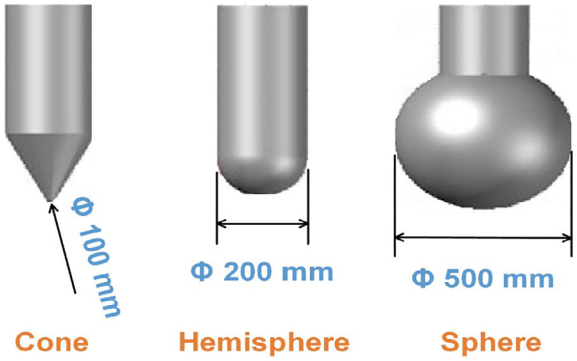


**Fig. 4.** Electrodes of three shapes at the high voltage side.

The $U_{50\%}$ breakdown voltage in the 1-m air gap under the positive lightning impulse voltage is about 540 kV. We set the applied voltage to ensure that the gap rarely reaches breakdown, but the streamer could initiate and propagate. A high-speed camera captures the configuration of the streamer discharge under lightning impulse voltages of different amplitudes, so we can obtain the streamer length. The sensor is placed on the axis of the 1-m rod–plate gap, because the sensor is sensitive in the axial direction, with the sensor at 30–70 cm above the ground.

## Analysis and measurement of Laplace electric field

We calculated the spatial distribution of the Laplace electric field in the 1-m rod–plate gap by using the charge simulation method (CSM). However, instead of using the CSM based on the uniqueness principle of the electric field, the free charge on the surface of the electrode, or the bound charge on the surface of the dielectric, we use a set of discrete charges called "simulated charges." For the three kinds of rod electrodes, due to the characteristics of the electrode structure with axial symmetry, a point charge, a line charge, a ring charge, and their combination are used to simulate the charge distribution on the surface of the electrode. To avoid damaging the electric field equation of the solved region, these charges should be set up outside the region; here, we set them inside the electrode.

Taking the hemisphere electrode as an example, the point charge $Q_0$ is set in the center of the hemisphere head of the electrode, and the line charge is set in the axis of the rod. We use $n-1$ roots of linear line charge of semi-infinite length at different initial positions to be superimposed. The density of the line charge is $\tau 1, \tau 2, \ldots \tau n-1$ respectively. Considering the influence of the earth, based on the mirror principle, in the symmetrical position, we set the charge of the same charge quantity and opposite polarity. Based on the CSM, $n$ matching points are gotten on the surface of the electrode, and the potential equation is given as:

$$PQ = \varphi \tag{1}$$

Among them,

$$Q = (\tau_1, \tau_2, \ldots \tau_{n-1}, Q_0)^T \tag{2}$$

$$P_{ij} = \frac{1}{4\pi\varepsilon} \ln \frac{z_j + z_i + \left[r_i^2 + (z_j + z_i)^2\right]^{1/2}}{z_j - z_i + \left[r_i^2 + (z_j - z_i)^2\right]^{1/2}} \begin{pmatrix} i = 1, 2, \ldots n \\ j = 1, 2, \ldots n-1 \end{pmatrix} \tag{3}$$

$$P_{in} = \frac{1}{4\pi\varepsilon} \left[ \frac{1}{\sqrt{r_i^2 + (z_0 - z_i)}} - \frac{1}{\sqrt{r_i^2 + (z_0 + z_i)}} \right] \tag{4}$$

In these equations, $z_j$ indicates the starting coordinate of each line charge, and $z_i$ and $r_i$ are the coordinates of the matching points on the electrode boundary. The potential and axial field strength at any point in the axial position of rod–plate gap can be obtained. In this calculation, the rod electrode potential is set to 1 kV. Fig. 6 gives us the calculated electric field distribution on the axis of the rod–plate gap for three different electrodes under a voltage of 1 kV.

As the sensor height decreases, the Laplace axis electric field of the three electrodes decreases gradually and tends to saturate. Around the electrode, compared with these, the axis electric field of the cone electrode is maximum, while that of sphere electrode is maximum far from the electrode.

To obtain the Laplace electric field, the lightning impulse voltage is applied to ensure that the air in the gap is not obviously ionized. The electric-field sensor is placed at a certain height in the axis direction of the 1-m rod–plate gap. To ease comparison, the measured electric fields are all converted to values under a voltage

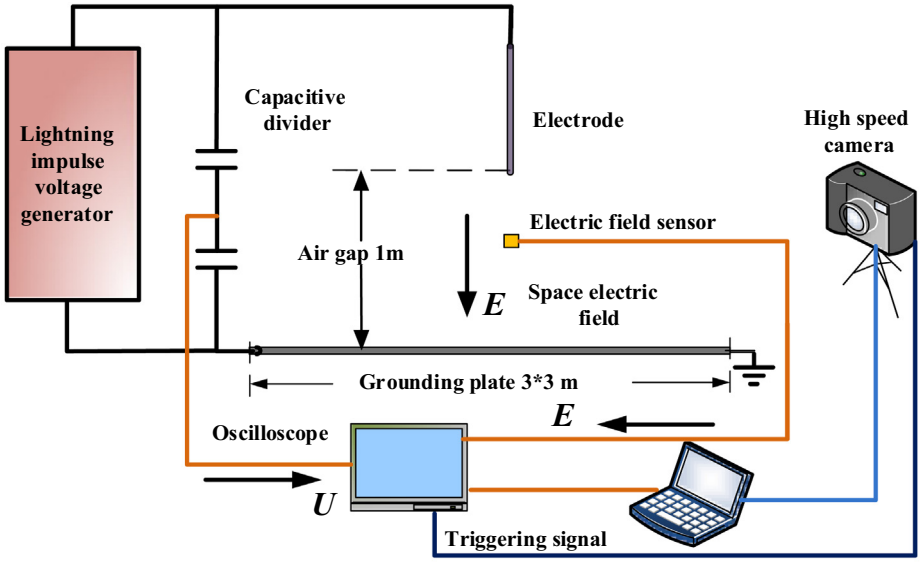


**Fig. 5.** Schematic of the experiment setup.

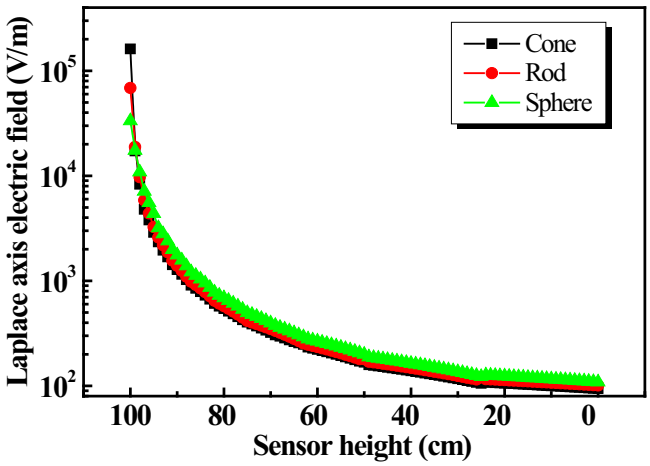


**Fig. 6.** Calculated axis direction electric field in the 1-m rod-plane gap.

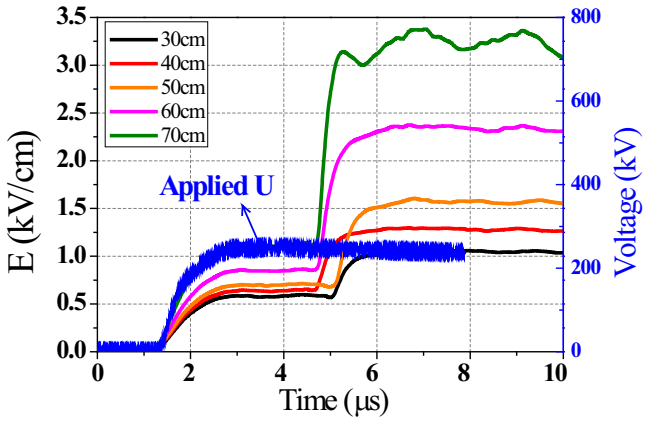


**Fig. 7.** Time-domain waves of the electric field distorted by space charge at sensor heights of 30–70 cm.

of 1 kV. Table 1 compares the calculated and measured Laplace axis electric field. The listed value at a given sensor height is the average of 20–30 measurements at the same applied voltage.

The measured results agree well with the calculated results. The error at most positions is within ±2%, though one position reaches +5%. This result shows that the electric-field sensor measures the space electric field accurately, with controllable error.

## Measurement of the Poisson electric field formed by space charge

At a sufficiently high applied impulse voltage, the measured electric field near the head of the rod electrode obviously deviates from the calculated value [19]. The time-domain waveform of the measured electric field has an obvious jump, and analysis of measurements suggests that the jump was caused by space charge [20]. The space charge generated by the streamer can be regarded as a whole, so the electric field of the external region is the superposition of the Laplace electric field generated by the applied voltage and the Poisson electric field generated by the space charge. The electric-field sensor measures the external field of the space charge region, reducing the impact of the space charge present on the sensor surface. Fig. 7 shows the typical measured electric field outside the space charge region.

Fig. 7 shows the output waveform of the electric-field sensor at various sensor heights. Here, the head curvature radius of the cone electrode is 2.5 cm, and the amplitude of the applied positive lightning impulse voltage is 200 kV. The electric-field sensor is placed outside the space charge region, as shown in Fig. 8. It was captured by a high-speed camera, as shown in Fig. 5. The camera can capture discharge images at the microsecond scale. The sensor is supported

**Table 1**
Comparison of calculated and measured Laplace electric fields, with various sensor heights in the axis direction.

| Sensor height (cm) | | 30 | 40 | 50 | 60 | 70 |
|---|---|---|---|---|---|---|
| Cone | Calculation (V/m) | 201 | 218 | 250 | 299 | 380 |
| | Measurement (V/m) | 208 | 217 | 255 | 297 | 372 |
| | Error % | 3.6 | −0.5 | 2 | −0.6 | −2 |
| Rod | Calculation (V/m) | 221 | 242 | 275 | 329 | 427 |
| | Measurement (V/m) | 223 | 255 | 278 | 324 | 436 |
| | Error % | 0.9 | 5.3 | 1.2 | −1.5 | 2.1 |
| Sphere | Calculation (V/m) | 274 | 299 | 338 | 411 | 548 |
| | Measurement (V/m) | 277 | 304 | 335 | 412 | 545 |
| | Error % | 1.4 | 1.5 | −0.8 | 0.2 | −0.5 |

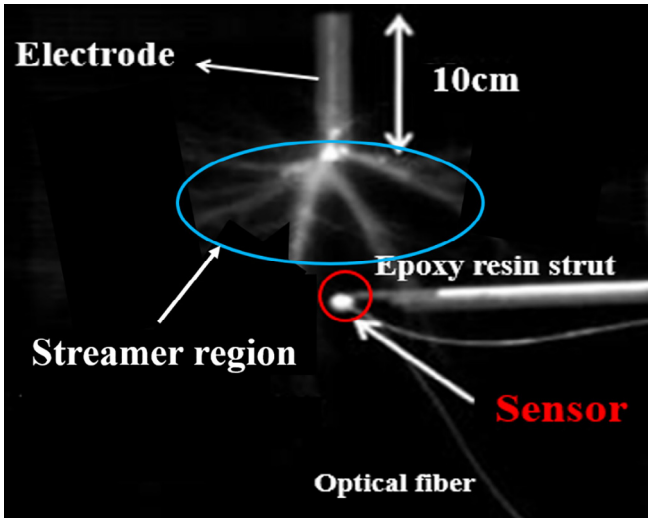


**Fig. 8.** Example of the space electric field measured by the field sensor, captured by a high-speed camera.

by an epoxy resin strut which is completely insulated and does not influence the space electric field. In Fig. 8, the shape of the tip of the rod electrode is spherical and the amplitude of the applied impulse voltage is 200 kV. Commonly, the sensor is located outside the streamer channel, which is hard to happen to be positioned inside the streamer channel, so it measures the space electric field.

By comparing the measured electric field with the applied lightning voltage at a sensor height of 70 cm, as the applied lightning voltage increases, the increases of voltage and electric field remain consistent. This result shows that the space electric field is initially only the Laplace electric field. After some time, the streamer seems to initiate, and space charge forms at the head of the electrode. This space charge distorts the space electric field because the new Poisson field superimposes over the original Laplace field. At this point, the time-domain waveform of the space electric field obviously increases. The field jump is caused by the space charge, and jump occurs when the streamer initiates. The waveforms in Fig. 7 were measured under the same applied lightning impulse voltage, so the initiation time of the streamer has some dispersion. Fig. 7 also shows that the amplitude of the electric field jump increases as the sensor height from the ground increases. Because the streamer channel has a certain density of space net charge and the charge density of the streamer head is the largest, the electric field of the region closer to the streamer head is greater.

## Discussion and analysis of the distorted electric field caused by space charge

*Quantitative analysis of the distorted electric field*

According to the results in the last section, the electric field caused by space charge is the field increment. To accurately obtain the distortion of the electric field, the results of three different electrodes are shown in Figs. 9–11. These results are measured at heights of 30–70 cm under an applied lightning impulse voltage at four amplitudes: 200, 230, 270, and 300 kV. Each data point is the amplitude of the field increment averaged from 20 to 30 measurements. The time between two discharges is several minutes, which is sufficient to ensure the full dissipation of space charges generated in the previous discharge as well as the surface charges that may attach to the sensor surface.

These figures show the increment amplitude of the electric field formed by the space charges on the axis of the 1-m rod–plate air gap. For the same rod electrode under the same lightning impulse voltage, the space electric field increases as the streamer region becomes closer to the space charge. For example, take the hemisphere electrode with the 1-cm head radius: when the sensor height increases from 30 cm to 70 cm, the space electric field increases by 1.8 kV/cm under an applied voltage of 200 kV. For a sensor with fixed height, as the lightning impulse voltage increases, the space electric field also significantly increases. The greater the applied voltage, the bigger the total space charge generated by the streamer discharge. In the meantime, the streamer region lengthens, so the space charge region gradually approaches the sensor. Thus, the measured space electric field distorted by space charge at the same position increases.

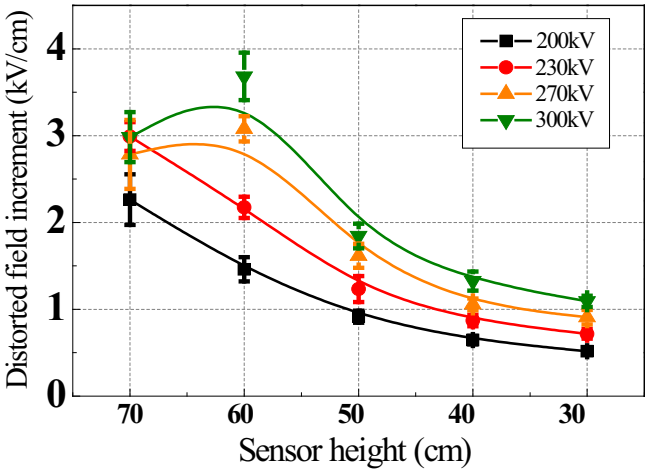


**Fig. 9.** Increment amplitude of electric field distorted by the space charge of the cone electrode.

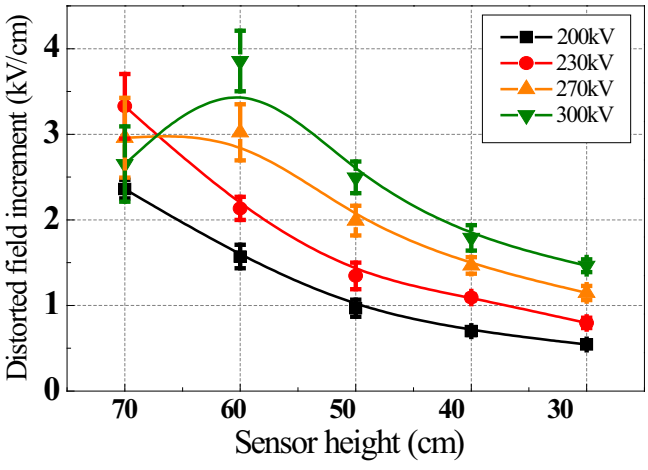


**Fig. 10.** Increment amplitude of electric field distorted by the space charge of the hemisphere electrode.

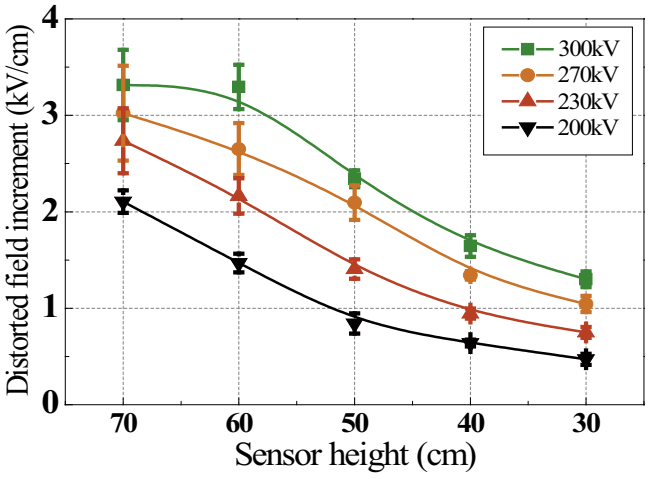


**Fig. 11.** Increment amplitude of electric field distorted by the space charge of the sphere electrode.

Fig. 12 shows that, for the hemisphere and cone electrodes at an applied voltage of 300 kV, the measured space charge field is less at a height of 70 cm than at 60 cm. This result is inconsistent with the previous analysis of the change regulation of the space charge electric field amplitude. The most likely reason for this inconsistency is that when the applied lightning impulse voltage is high enough, the streamer propagates intensely, so the length of the streamer region becomes greater than 30 cm, and at this time the sensor, at a height of 70 cm, should be inside the space charge region. The charge density of the streamer head is very high and the electric field of streamer head is huge, reaching more than 100 kV/cm [21]. As the sensor approaches the head of the streamer, the measured field becomes bigger and bigger. Once the sensor is inside the streamer region, the sensor changes to measure the electric field inside the streamer channel. However, the electric field of the streamer channel is far less than that of the streamer head, which is generally considered to be 4–5.5 kV/cm for long air gap

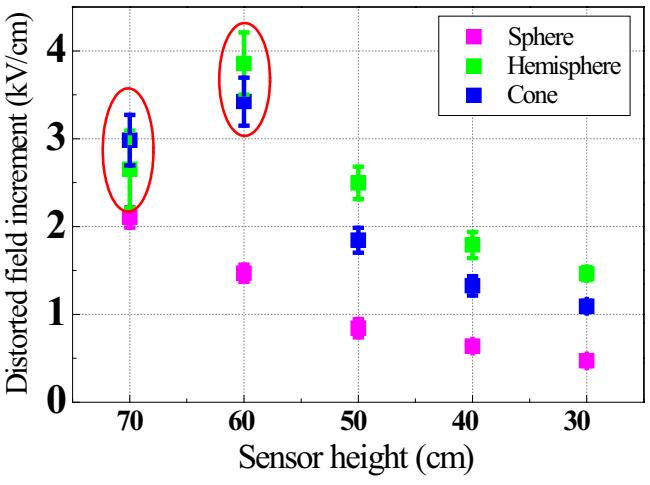


**Fig. 12.** Increment amplitude of electric field distorted by space charge for various electrodes under a lightning impulse voltage of 300 kV.

discharge [22]. Thus, the electric field measured at a height of 70 cm is most likely the streamer channel electric field, which is smaller than that at a height of 60 cm. Fig. 13 shows the various streamer region lengths of the cone electrode under various applied lightning impulse voltages, captured by a high-speed camera.

The average distorted electric field measured at a height of 70 cm is 3.45 kV/cm, averaged from 25 measurements using the cone electrode under the 300-kV lightning impulse voltage. This electric field is slightly smaller than the electric field of the streamer channel. This behavior occurs because when the sensor is placed in a relatively strong impulse electric field, a fraction of space charge inevitably accumulates on the surface of the electric field sensor, and this surface space charge can further distort the electric field. Although we have not yet quantified the effects of this cumulative charge, our electric-field sensor provides a more reliable method to directly measure the streamer channel field, which will be key in later research.

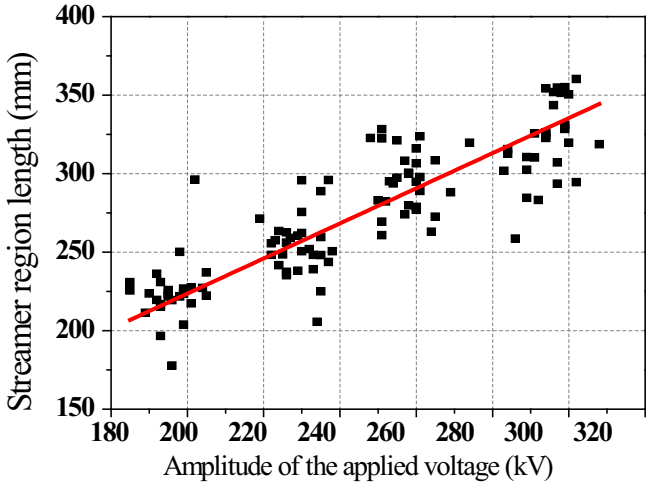


**Fig. 13.** Length of the streamer region as a function of the amplitude of the applied lightning impulse voltage.

*Compared with results calculated by the analytical model*

The model of streamer space charge has been widely researched. Early Dawson-Winn [27] used the point charge to simulate the space charge concentrated at the head of the streamer in order to study on the possibility which the streamer developed into the low electric field region. Goelian [7] thought that the space charge region consisted of N same streamers and uniformly distributed cylindrical charges were used to simulate branches of the streamer. The research group of Cooray has established the static model of the space charge [8]. They assumed the streamer region was a cone and adopted many groups of annular charges to simulate the streamer region. They have calculated the distribution of the charge density in the streamer region based on the consideration that the field inside the streamer region was the field of the stable development of streamer. In this paper, the distribution of the space charge density is considered as a function of spatial coordinates and the model of the space charge has been established. On the basis of those, the axial electric field on the axis of rod-plate gap can be calculated.

The space charge region of streamer is equivalent to a part of the space sphere emitted from the tip of the rod electrode, as shown in Fig. 14.

The sphere takes the tip of the rod electrode as its origin. Its radius $L$ is the length of the streamer region and the solid angle $\Omega$ describes the size of the space charge region. $\Omega$ has the following relationship with the plane angle $\alpha$:

$$\Omega = 2\pi(1 - \cos\alpha) \tag{5}$$

The space charge of the streamer region can be regarded as a continuous distribution and the electric field inside the streamer region is well distributed. The spherical coordinate system is established by taking the tip of the rod electrode as the origin of coordinate. The space charge density can be expressed as below:

$$\rho(r, \varphi, \theta) = \frac{A}{r} \tag{6}$$

Among them, $A$ is a constant, $A = 2\varepsilon_0 E_s$, and $E_s$ is the field of streamer. For the rod-plate gap, the electric potential at any point on the axis can be expressed as:

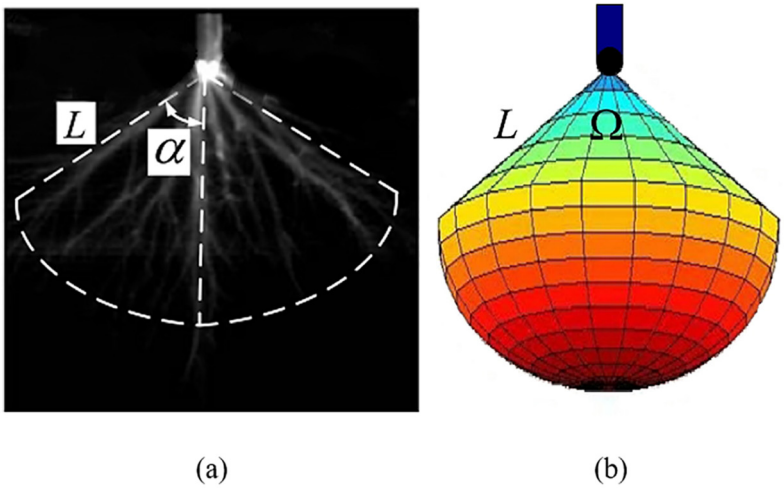


(a) Photo of streamer discharge taken by the high speed camera

(b) Space charge model based on a part of a sphere

**Fig. 14.** Space charge region of the model.

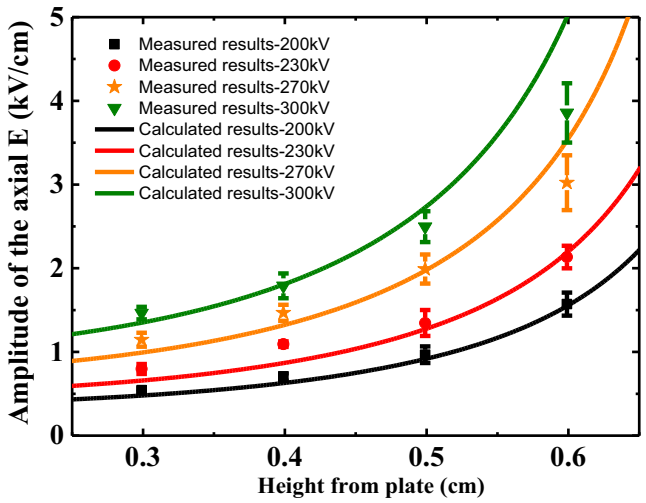


**Fig. 15.** Comparison between calculated and measured amplitudes of the axial electric field on the axis of the 1 m rod-plate gap under different applied impulse voltages.

$$\varphi(\vec{r}) = \varphi_L(\vec{r}) + \frac{1}{4\pi\varepsilon_0}\int\int\int_V \frac{\rho(r,\varphi,\theta)}{|\vec{r}-\vec{r}'|}dV \tag{7}$$

Thereinto, $\varphi_L(\vec{r})$ is the background potential, which is determined by the applied voltage. $\rho(\vec{r})$ is the space charge density, $\vec{r}'$ is origin coordinate and $\vec{r}$ is coordinate of target point. $V$ is the volume of the space charge region. From the relation between electric field and electric potential, the space field at any point is:

$$E(\vec{r}) = E_L(\vec{r}) + \frac{1}{4\pi\varepsilon_0}\sum\frac{\rho(r,\varphi,\theta)\,\vec{e}}{|\vec{r}-\vec{r}'|^2} \tag{8}$$

$\vec{e}$ is unit vector. $E_L(\vec{r})$ is Laplace electric field and the jump part of an electric field can be calculated by the second term on the right side of the Eq. (8). This equation is limited to the calculation of the electric field at a certain point outside space charge region.

For the rod electrode with a tip radius of 1 cm, according to the configuration of the captured streamer discharge in experiments, the length of the streamer region is 20–30 cm and the plane angle of that is in the range of 40–80 degrees. In this paper, the amplitude of the axial electric field outside the space charge region on the axis of the 1 m rod-plate gap is calculated by using the above model. In the calculation, we assume that $L$ is 25 cm and $\alpha$ is 60 degrees. As shown in Fig. 15, the comparison between calculated and measured results is presented.

Overall the calculated values are in good agreement with the measured values. Also from that figure, when the applied impulse voltage is great enough, there are several differences between the calculated and measured values at some positions close to the rod electrode. In the calculation, the length of the space charge region is assumed to be 25 cm and the points on the curves are all outside the space charge region. In fact, under 300 kV impulse voltage, the obtained streamer length can reach 35–40 cm. So the sensor is very close to the space charge region or inside the space charge region. Because the space charges can adhere to the surface of the sensor, the measured electric field is often smaller than the actual value.

## Conclusions

We used an electric-field sensor to measure the Poisson electric field produced by space charge and the Laplace electric field on the axis of the 1-m rod–plate gap under positive lightning impulse voltage. We compared these measurements to calculated results from CSM, finding that our sensor accurately, quantitatively measured the changing space electric field. When the sensor is outside the space charge region, the measured electric field is the superposition of the Laplace electric field, generated by capacitive voltage between electrodes, and the Poisson electric field, generated by space charge. The time-domain waveform shows that an obvious jump occurred at the inception time of the streamer, and the amplitude of the jump is the distorted electric field generated by space charge. Also, the closer the streamer region is to the space charge, the greater the amplitude of the distorted electric field becomes. When the streamer region is long enough, the sensor should be located inside the streamer channel. Because the space charges can adhere to the surface of the sensor, the measured electric field is often less than 4 kV/cm. We established the space charge model to calculate the distorted electric field in space. The accuracy of the measured results can be confirmed by compared the calculated and measured values. At present, the electric field of the streamer channel can only be measured by using spectral technology [23–25]. However, spectral measurement of streamer discharge often has limited accuracy [26]. If we can quantify the impact of the surface charges of the sensor on the measured results in the future, our sensor can provide another way to directly measure the streamer electric field. This will be the focus of our future research.

## Acknowledgments

This work is supported by the National Natural Science Fund Program under grants 51325703, 51377094, 51407102, and 51577098.

## References

[1] Liu ZY. External insulation of UHV AC transmission system. Beijing: China Electric Power Press [in Chinese].
[2] The Renardières Group. Research on long air gap discharges at Les Renardières. Electra 1972;29:53–157.
[3] The Renardières Group. Research on long air gap discharges at Les Renardières – 1973 results. Electra 1974;35:49–156.
[4] The Renardières Group. Positive discharges in long air gap discharges at Les Renardières – 1975 results. Electra 1977;53:31–153.
[5] The Renardières Group. Negative discharges in long air gap discharges at Les Renardières. Electra 1981;74:67–216.
[6] Gallimberti I. A computer model for streamer propagation. J Phys D 1972;5:2179–89.
[7] Goelian N, Lalande P, et al. A simplified model for the simulation of positive-spark development in long air gaps. J Phys D: Appl Phys 1997;20:2441–52.
[8] Becerra M, Cooray V. A self-consistent upward leader propagation model. J Phys D: Appl Phys 2006;39(16):3708–15.
[9] Feser K. A potential free spherical sensor for the measurement of transient electric field. IEEE Trans Power Deliv 1984;103(10):2904–11.
[10] Bulmer CH, Burns WK, Moeller RP. Linear interferometric waveguide modulator for electromagnetic-field detection. Opt Lett 1980;5(5):176–8.
[11] Bulmer CH, Burns WK. Linear interferometric modulators in Ti: $LiNbO_3$. J Lightwave Technol 1984;LT-2(4):512–21.
[12] Hidaka K, Fujita H. A new method of electric field measurements in corona discharge using Pockels device. J Appl Phys 1982;53(2):5999–6003.
[13] Hidaka K, Murooka Y. Electric field measurements in long gap discharge using Pockels device. IEE Proc 1985;132(3):132–46.
[14] Rong Zeng, Weiyuan Chen, Jinliang He, et al. Study on optical electric integrated electric field measurement system and application in high voltage measurement. High Volt Eng 2006;32(7):1–5 [in Chinese].
[15] Ben Niu, Rong Zeng, Yinan Geng, et al. Electric field measurement of switching impulse discharge in UHV tower. High Volt Eng 2009;35(4):731–5 [in Chinese].
[16] Zeng R, Zhang Y, et al. Measurement of electric field distribution along composite insulators by integrated optical electric field sensor. IEEE Trans Dielectr Electr Insul 2008;15(1):302–10.
[17] Zeng R, Wang B, et al. Design and application of an integrated electro-optic sensor for intensive electric field measurement. IEEE Trans Dielectr Electr Insul 2011;18(1):312–9.
[18] Wang Z, Geng Y. Study on the streamer inception characteristics under positive lightning impulse voltage. AIP Adv 2017;7(11):115115.

[19] Ben Niu. Research on integrated electro-optical time domain electric field sensor for intensive electric field [D]. Beijing: Tsinghua University; 2008 [in Chinese].
[20] Zeng R, Zhuang CJ, et al. Electric field step in air gap streamer discharges. Appl Phys Lett 2011;99:221503.
[21] Aleksandrov NL, Bazelyan EM. Simulation of long-streamer propagation in air at atmospheric pressure. J Phys D Appl Phys 1996;29(3):740–52.
[22] Allen NL, Mikropoulos PN. Dynamics of streamer propagation in air. J Phys D Appl Phys 1999;32(8):913–9.
[23] Pancheshnyi S, Sobakin S, Starikovskaya S, Starikovskii A. Discharge dynamics and the production of active particles in a cathode-directed streamer. Plasma Phys Rep 2000;26:1054–65.
[24] Kozlov K, Wagner H, Brandenburg R, Michel P. Spatio-temporally resolved spectroscopic diagnostics of the barrier discharge in air at atmospheric pressure. J Phys D: Appl Phys 2001;34:3164–76.
[25] Bonaventura Z, Bourdon A, Celestin S, et al. Electric field determination in streamer discharges in air at atmospheric pressure. Plasma Sources Sci Technol 2011;20(3):035012.
[26] Naidis GV. Positive and negative streamers in air: velocity–diameter relation. Phys Rev E 2009;79:057401.
[27] Dawson GA, Winn WP. A model for streamer propagation. Phys Astron 1965;183(2):159–71.
[28] Zeng Rong, Zhuang Chijie, Zhou Xue, et al. Survey of recent progress on lightning and lightning protection research. High Volt 2016;1(1):2–10.
[29] Zhuang Chijie, Zeng Rong. A local discontinuous Galerkin method for 1.5-dimensional streamer discharge simulations. Appl Math Comput 2013;219(19):9925–34.
[30] Chen She, Zeng Rong, Zhuang Chijie, et al. Switching impulse breakdown characteristics of large sphere-plane air gaps compared with rod-plane air gap. IEEE Trans Dielectr Electr Insul 2013;20(3):839–44.
[31] Zhuang Chijie, Zeng Rong, Zhang Bo, et al. 2-D discontinuous Galerkin method for streamer discharge simulations in Nitrogen. IEEE Trans Magn 2013;49(5):1929–32.
[32] Zhuang Chijie, Liu Hanbo, Zeng Rong, et al. Adaptive strategies in the leader propagation model for lightning shielding failure evaluation: implementation and applications. IEEE Trans Magn 2016;52(3):9400604.